

cambridge.org/mrf

Navneet Kaur¹ , Jagtar Singh Sivia² and Rajni³

¹Department of Electronics and Communication Engineering, Punjabi University, Patiala, Punjab, India; ²YCoE, Punjabi University Guru Kashi Campus, Talwandi Sabo, Bathinda, Punjab, India and ³Shaheed Bhagat Singh State Technical Campus, Ferozepur, Punjab, India

Research Paper

Cite this article: Kaur N, Sivia JS, Rajni (2022). Design of frequency reconfigurable planar antenna using artificial neural network. *International Journal of Microwave and Wireless Technologies* **14**, 1107–1118. <https://doi.org/10.1017/S1759078721001434>

Received: 15 May 2021

Revised: 11 September 2021

Accepted: 18 September 2021

First published online: 14 October 2021

Keywords:

Artificial electromagnetic materials; artificial neural network; metamaterial; metasurface superstrate; reconfigurable antenna; S-parameters; wireless communications

Author for correspondence:

Navneet Kaur,

E-mail: navsandhu31696@gmail.com

Abstract

In this paper, the design of frequency reconfigurable planar antenna by incorporation of metasurface superstrate (FRPA-MSS) is presented using an artificial neural network. The dual-layer radiating structure is created on a 1.524 mm thick Rogers RO4350B substrate board ($\epsilon_r = 3.48$, $\tan \delta = 0.0037$). The candidate antenna is designed and analyzed using a high-frequency structure simulator (HFSS) tool. The transfer matrix method is employed for the successful retrieval of electromagnetic properties of the metamaterial. Frequency reconfiguration is achieved by placing the metasurface superstrate onto the rectangular patch antenna. A simplified ANN approach has been employed for the design of metasurface incorporated proposed antenna. Presented prototypes are characterized through experimental measurements. It is found from the practical observations that the proposed antenna effectively reconfigures the tuning range from 5.03 to 6.13 GHz. Moreover, the presented antenna operates efficiently with agreeable gain, good impedance matching, and stable pattern characteristics across the entire operational bandwidth. The experimental results obtained validate the simulated performance.

Introduction

In the present scenario, reconfigurable antennas have grabbed huge attention from the research community due to their ability to integrate multiple standards into a single platform [1]. Therefore, the wireless systems are empowered with reconfigurable antennas to enhance the overall performance and providing cost-effective solutions [2]. The important characteristics that are to be considered while designing these antennas are operating frequency, polarization, and radiation pattern [3]. Modern-day wireless communication systems such as mobile phones, laptops, watches, tablets, etc. support several wireless standards. To fulfill such requirements, multiband, wideband and frequency reconfigurable antennas are the probable choices. Frequency reconfigurable or tunable antennas act as the best alternative by opening up new horizons, thereby providing additional functionality levels [4]. These antennas can change their operating frequency while maintaining stable polarization and radiation pattern modes over the entire frequency range [5]. This feature is accomplished by redistributing the surface current within the radiating element by employing positive intrinsic negative (PIN) diode [6], varactor diode [7], radio frequency micro-electro-mechanical system (RF-MEMS) switches [8], multi-reed switches [9], and optical element [10]. Numerous reconfigurable antennas have been demonstrated based on different switching techniques. In [11], the spiral-shaped flexible and compact frequency reconfigurable antenna is implemented for wireless applications. Ouyang *et al.* [12] proposed a microstrip patch antenna with an electronically steerable parasitic array radiator. With the employment of switches and biasing networks, the non-linear effects and insertion loss increase, that in turn, degrades the performance of an antenna.

Over the previous decades, artificial materials have garnered prodigious attention in designing smart antenna structures with improved performance parameters [13]. The origination of metamaterial reveals an outstanding achievement in comparison to conventional materials. This idea first came into existence in 1967 [14]. After that, the concept of metamaterial has been explored widely to provide a wide tuning range, thus offering a promising solution to various research-oriented problems. The remarkable electromagnetic properties of metamaterial such as negative refractive index, permittivity, and permeability values, anti-parallel phase and group velocities, etc. are responsible for designing fascinating antenna structures with superior characteristics [15]. Ramachandran *et al.* [16] proposed a left-handed metamaterial design for satellite applications constructed using a combination of circular and square ring structures. Though the three-dimensional metamaterial is a young field and has achieved blooming technological advancements in several research areas such as microwaves and infrared regions yet they lack paucity in realizing lossless optical metamaterials. Thus to provide easy fabrication, two-dimensional metasurfaces have emerged out as a multifaceted branch

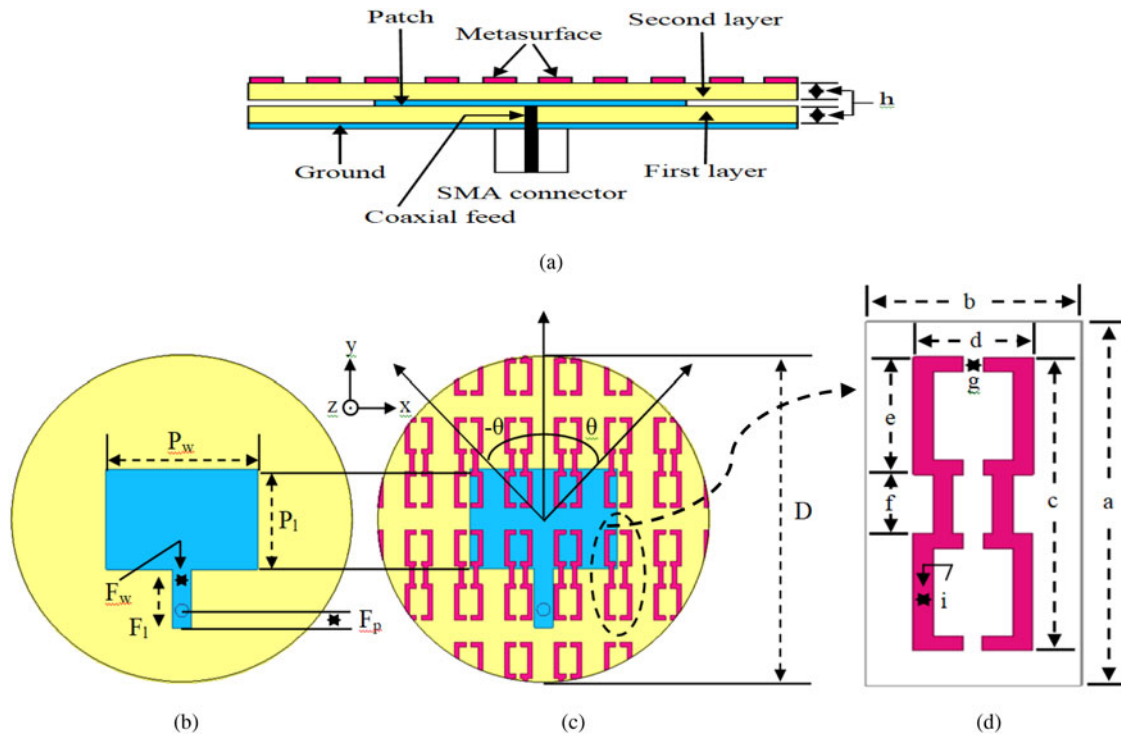


Fig. 1. Design schematic of FRPA-MSS (a) dual-layer module (b) patch antenna (c) metasurface, and (d) zoomed version of a unit cell.

Table 1. FRPA-MSS design specifications.

Parameters	D	h	P_l	P_w	F_l	F_w	F_p	a	b	c	d	e	f	g	i
Values (mm)	36	1.524	11	16	6.5	2	2	12.4	5.4	10	3	4	2	0.5	0.5

of engineering science in the last decade [17]. The surface variant of metamaterial is portrayed as metasurface which means a surface distribution of small apertures or holes [18]. Metasurfaces (MS) are uniformly arranged, two-dimensional planar periodic structure that is analogous to three-dimensional metamaterials [19]. A metasurface-based planar frequency reconfigurable antenna is designed with a fractional tuning range of 14.6% [20]. The frequency reconfigurable slot antenna is demonstrated using a single-layer metasurface [21]. Majumder *et al.* [22] proposed a frequency reconfigurable antenna by loading two metasurface layers onto the slot antenna. Frequency and polarization reconfigurable antenna is designed using polarization conversion metasurface [23]. Metasurface enabled mechanically frequency reconfigurable antenna by an equivalent radially homogenous model is demonstrated by Li *et al.* [24]. Singh *et al.* demonstrated the designing and analysis of circular fractal antenna using artificial neural networks (ANNs) [25]. Kaur *et al.* presented metasurface incorporated frequency reconfigurable antenna and used ANN approach to develop antenna [26, 27].

By thoroughly reviewing the aforementioned literature, the design of frequency reconfigurable planar antenna is presented using an ANN with enhanced performance characteristics. First, the designing process of a metasurface incorporated dual-layer frequency reconfigurable antenna is illustrated. Then the specific characteristics of metamaterial are analyzed. Afterwards, the ANN framework is illustrated. Followed by this, the results are discussed. In the end, the conclusion is presented.

Designing process of frequency reconfigurable antenna

The proposed work utilizes a dual-layer approach for implementing the frequency reconfigurable antenna. The schematic of the design is illustrated in Fig. 1. The dual-layer module is composed of two substrate layers as shown in Fig. 1(a). The rectangular-shaped patch antenna and circular ground plane are imprinted on the upper and lower side of the first layer, respectively. The periodical array of compounded double split-ring resonator (CDSRR) shaped unit cells forming the metasurface is printed on the upper side of the second layer. This module uses a flexible Rogers RO4350B substrate with a dielectric constant (ϵ_r) of 3.48 and loss tangent ($\tan \delta$) of 0.0037. A fixed thickness of 1.524 mm has opted for both layers, thus the total thickness is 3.048 mm. For the excitation purpose, a 2 mm wide feedline is used that provides a characteristic impedance of 50 Ω . The antenna is fed directly using coaxial feed and the SubMiniaturized version A (SMA) connector is used for connecting purposes. The overall dimensions of the structure are $D \times 2(h)$ mm². For proper matching conditions, both the layers are taken in circular form. The angle θ , the orientation angle of the metasurface, is measured with respect to the y-axis in a clockwise and anticlockwise direction and the maximum orientation angle is 90°. The schematic of the patch antenna and metasurface is demonstrated in Figs 1(b) and 1(c), respectively. The zoomed version of the unit cell is represented in Fig. 1(d). The optimized parametric design specifications of the proposed antenna are listed in Table 1.

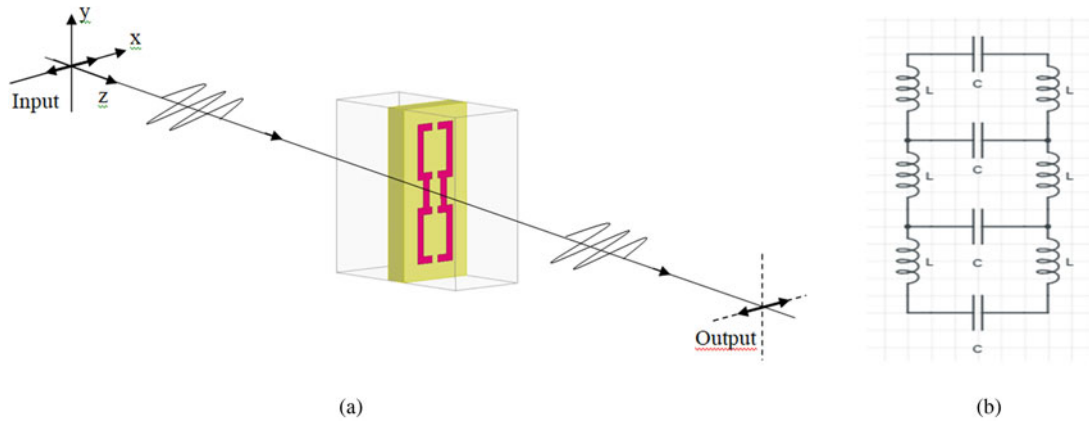


Fig. 2. Analysis of CDSRR (a) waveguide medium for extracting the S-parameters and (b) equivalent circuit of the unit cell.

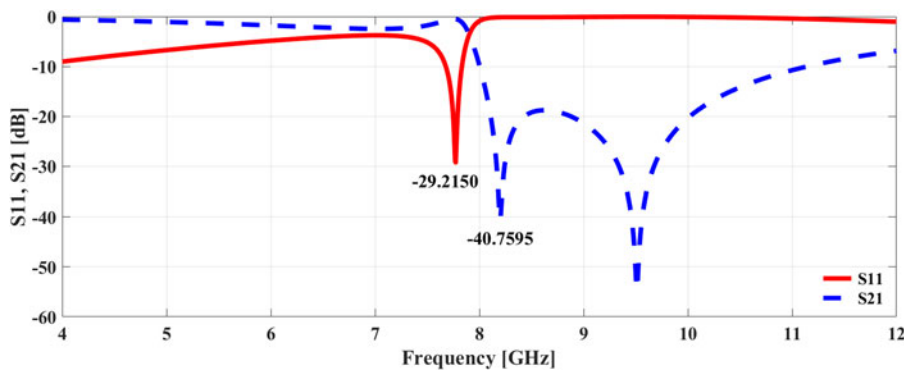


Fig. 3. Extracted S11 and S21 of the proposed unit cell structure.

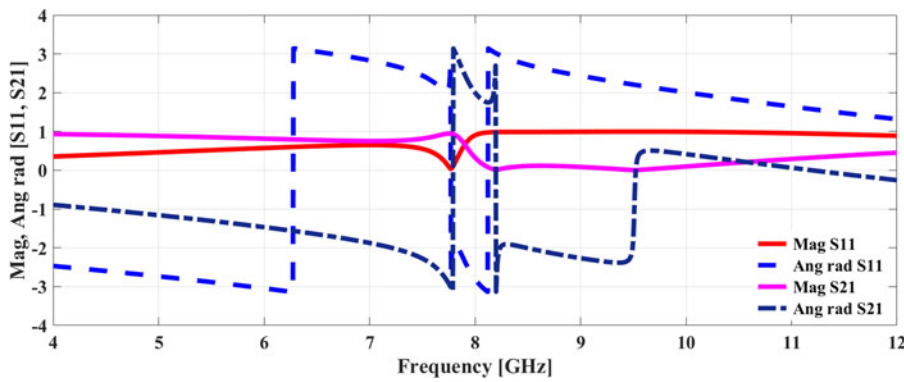


Fig. 4. Magnitude and phase characteristics of S11 and S21.

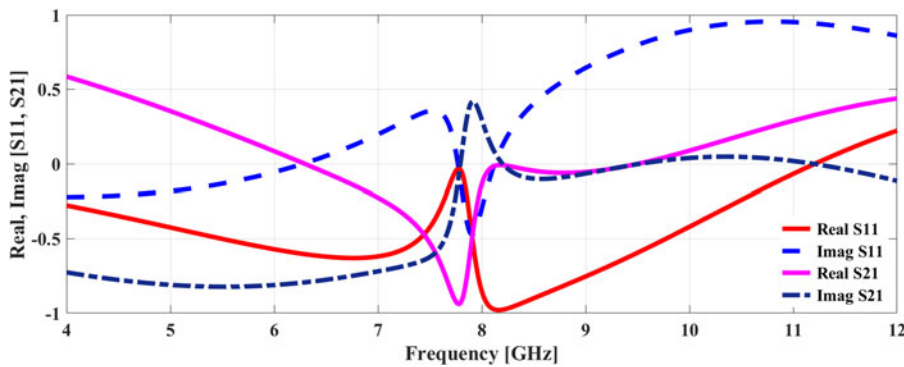


Fig. 5. Real and imaginary parts of S11 and S21.

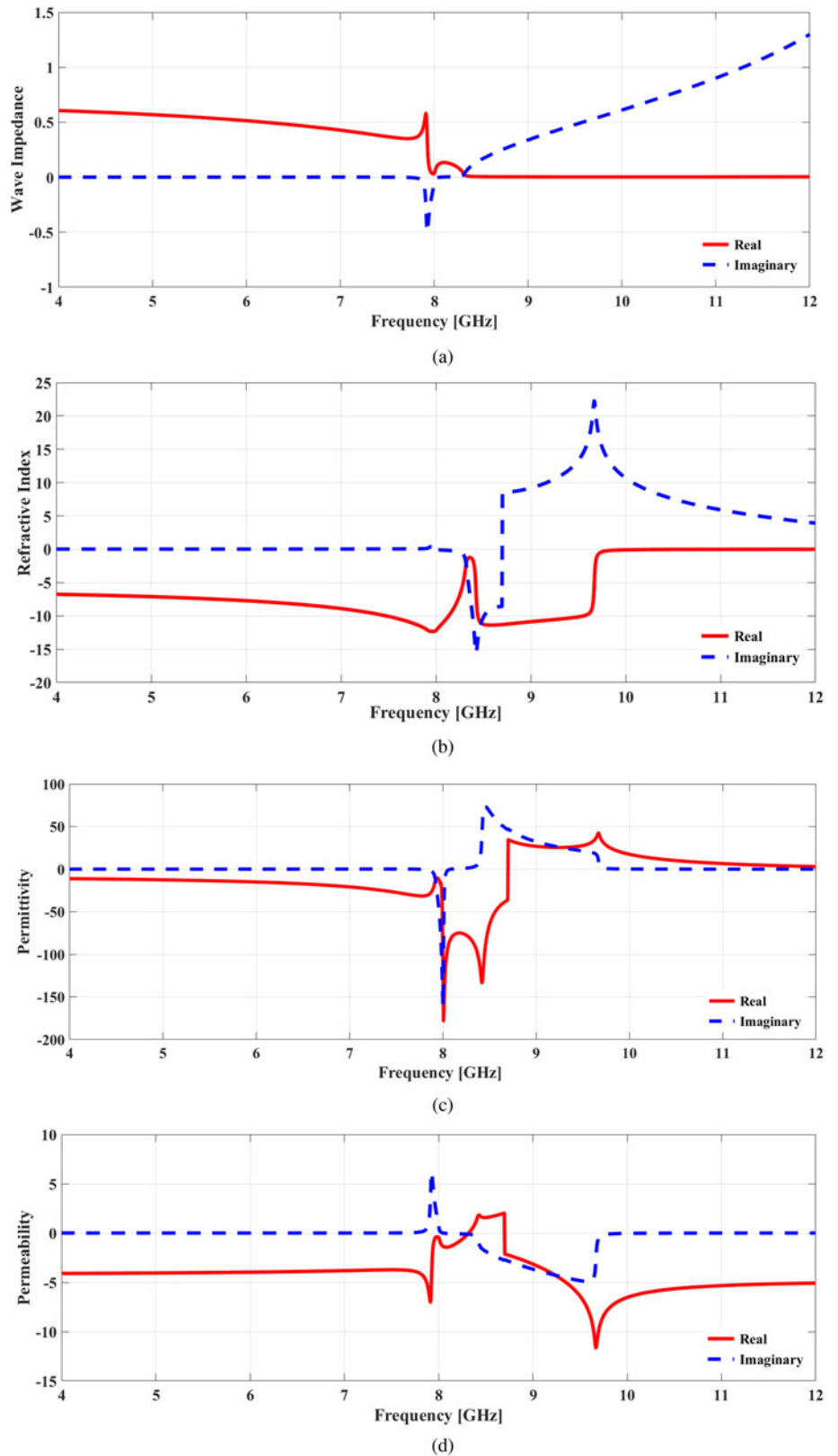


Fig. 6. Effective values of homogenous parameters (a) wave impedance (b) refractive index (c) permittivity, and (d) permeability.

Analysis of metamaterial

The effective electromagnetic parameters (permittivity ϵ_{eff} /permeability μ_{eff} /refractive index n_{eff}) of the unit cell structure are extracted by utilizing the scattering parameters. For this, the

whole setup is placed inside the waveguide environment with ports, electric field, and magnetic field applied along the respective axis [28–31]. This waveguide medium is shown in Fig. 2(a). The structure functions like an LC resonator with a gap and

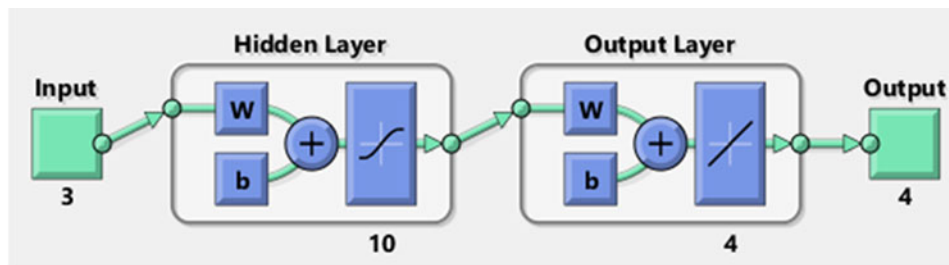


Fig. 7. Proposed FFBPN model.

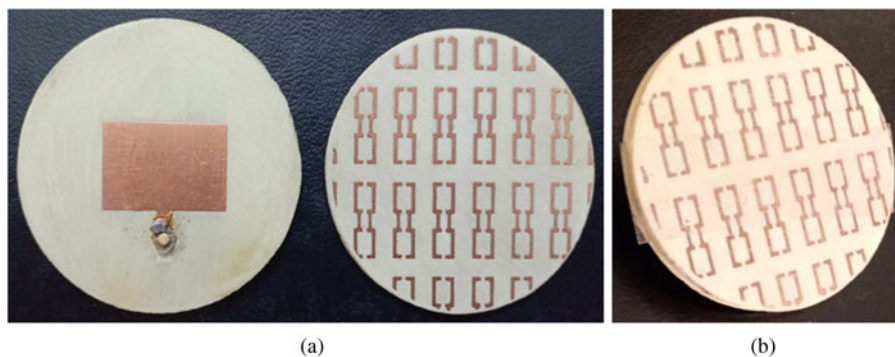


Fig. 8. Photographic view of the fabricated antenna using RO4350B substrate (a) patch antenna and metasurface and (b) FRPA-MSS.

metal strip corresponds to capacitive and inductive elements, respectively. The LC equivalent circuit of the unit cell is depicted in Fig. 2(b).

Figure 3 shows the extracted reflection (S11) and transmission (S21) coefficient of the unit cell structure. It is evaluated that a strong reflection of -29.2 dB is observed at 7.7 GHz. This frequency points to the coexistence of electric and magnetic resonances [32]. The first transmission minimum is -40.7 dB at 8.2 GHz. The magnitude and phase characteristics of the reflection and transmission coefficient are delineated in Fig. 4. From these results, the phase reversal property of metamaterial is demonstrated. The real and imaginary parts of the reflection and transmission coefficient are described in Fig. 5. Further, results are imported to Matrix Laboratory (MATLAB) for determining the electromagnetic properties of metamaterial.

$$z = \sqrt{\frac{(1 + S_{11})^2 - S_{21}^2}{(1 - S_{11})^2 - S_{21}^2}} \tag{1}$$

$$n = \frac{1}{kd} \cos^{-1} \left[\frac{1}{2S_{21}} (1 - S_{11}^2 + S_{21}^2) \right] \tag{2}$$

Different techniques have been employed so far for extracting the notable properties of metamaterial. Nicolson Ross Weir (NRW) and the transfer matrix method are popular as they are based on two-port analysis [33]. In this work, the transfer matrix method is employed as this is a direct method for determining the wave impedance. The wave impedance and refractive index are determined using (1) and (2), respectively. Here, z and n symbolize the wave impedance and refractive index, respectively. The literal k and d represent the wave number of the incident wave and thickness of the dielectric slab, respectively. The permittivity and

Table 2. Performance evaluation of ANN analysis.

	Samples	MSE	Regression
Training	26	2.76710×10^{-4}	9.99979×10^{-1}
Validation	5	6.27304×10^{-4}	9.99952×10^{-1}
Testing	5	1.95663×10^{-4}	$9.99984e \times 10^{-1}$

permeability values can be attained using (3) and (4).

$$\epsilon = \frac{n}{z} \tag{3}$$

$$\mu = nz \tag{4}$$

The material characteristics of the metamaterial are determined from the negative parts of permeability and permittivity. Thus, reflection and transmission are the integral parts of the said method. Figure 6 illustrates the effective values of homogeneous parameters in the desired frequency range. The bold red line represents the real part and the dashed blue line indicates the imaginary part of the associated parameter. The positive real value of wave impedance exists from 4 to 8.5 GHz range. Similarly, the negative real value exhibited by permittivity exists in 4–8.47 GHz and permeability in 4–8.2 GHz and 8.46–12 GHz. The permittivity and permeability values show electric and magnetic plasma frequencies. The refractive index shows its negative real value in between the electric and magnetic plasma frequencies. The successful retrieval of results in the 4–8.2 GHz frequency range confirms that the aforementioned structure exhibits left-handed properties of metamaterial. This in turn shows the effectiveness of the designed approach.

The analysis of the mathematical model of an equivalent circuit of CDSRR [34] is determined using (5)–(9). The equations

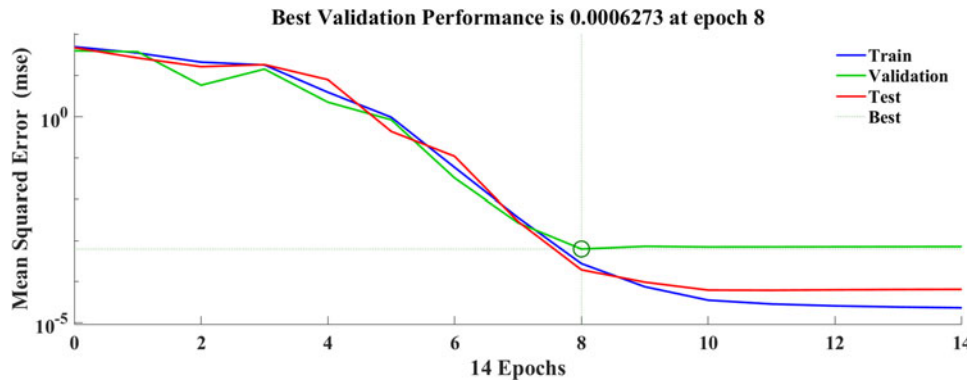


Fig. 9. Performance plot for analyzing the designed antenna.

have been modified as a single ring has been considered in the proposed design.

$$L^{CDSRR} = \frac{\mu_0 I_{avg}^{CDSRR}}{2} \frac{1}{4} \left[\ln \left(\frac{I_{avg}^{CDSRR}}{i} \right) - 2 \right] \tag{5}$$

$$I_{avg}^{CDSRR} = 4l - 4g \tag{6}$$

$$C^{CDSRR} = 2\epsilon_0 \epsilon_r^{sub} \frac{2i + g\sqrt{2}}{\pi} \operatorname{arccosh} \left[\frac{2i + g}{g} \right] \tag{7}$$

$$\epsilon_r^{sub} = 1 + \frac{2}{\pi} \operatorname{arctg} \left[\frac{h}{2\pi i} \right] (\epsilon_r - 1) \tag{8}$$

$$f = \frac{1}{2\pi\sqrt{L^{CDSRR}C^{CDSRR}}} \tag{9}$$

where, L^{CDSRR} and C^{CDSRR} are the inductance and capacitance of the equivalent circuit, respectively. μ_0 and ϵ_0 are the absolute permeability and permittivity, respectively. I_{avg}^{CDSRR} and ϵ_r^{sub} are the average length of the unit cell and relative permittivity of the substrate. ϵ_r and f represent the relative permittivity of material, and the analytical frequency, respectively. From the equations, it is evaluated that the analytical results show a frequency of 7.9 GHz that matches nearly its full wave simulated results.

Artificial neural network

It is imperative to design the metasurface unit cell precisely as the metallic loop represents inductance L, and the gap between them represents capacitance C, which in turn decides the resonating frequency of the unit cell. Thus the resonance can be controlled by changing the geometry of the structure. Therefore, an ANN has been developed for the analysis of metasurface and incorporated in antenna for reconfiguration.

ANN is a powerful data computational tool that analyzes and processes information in a similar way the human brain does. It also plays a crucial role in the designing and analysis of an antenna [35, 36]. The basic unit that acts as the building block of the neural network is an artificial neuron. The feed-forward

back propagation network (FFBPN) is made up of many interconnected neurons that are organized in three layers: input, hidden, and output layer [37]. The information flows from the input layer to the output layer after progressing through one or more hidden layers. Each neuron is connected to other neurons via direct communication links with an individual weight connected to each link. The difference between the desired output and network output generates an error signal. Thus, ANN can adapt, learn and recollect the information just like a biological neural network [38]. The proposed FFBPN model is elucidated in Fig. 7. This model is constructed using three input layer neurons, four output layer neurons, and 10 hidden layer neurons. The unit cell dimensions and orientation angle of a frequency reconfigurable planar antenna by incorporation of metasurface superstrate (FRPA-MSS) are considered as inputs and their resonant frequencies are considered as output. To evaluate this process, a data set consisting of 36 samples is created through parametric analysis. From this total, the training set contains 26 samples, five samples in the validation set, and five samples in the testing set.

Results and discussion

The finite element method (FEM)-based 3D full-wave HFSS support tool is deployed for simulating the antenna prototype. The photographic view of the fabricated prototype is shown in Fig. 8. Anritsu MS2028C vector network analyzer (VNA) is used for evaluating the experimental results.

ANN results

A data set containing 36 samples is created by changing the basic dimensions of unit cell and the value of rotation angle for training the ANN model. For this purpose, the input parameters considered are “c”, “d”, and “θ”, and output parameters are “ f_{r1} ”, “ f_{r2} ”, “ f_{r3} ”, and “ f_{r4} ”. The desired degree of accuracy is achieved using the Levenberg–Marquardt algorithm. The training function employed is trainlm. Tansig and purelin are the transfer functions used in the hidden and output layers, respectively. The output of the model is evaluated using three main statistical parameters mean squared error (MSE), number of epochs used, and maximum absolute error. The performance evaluation for analyzing the designed antenna is described in Table 2. The performance plot for analyzing the designed antenna is illustrated in Fig. 9. It is noticed in plot that best validation performance takes place at 0.0006273 at epoch 8.

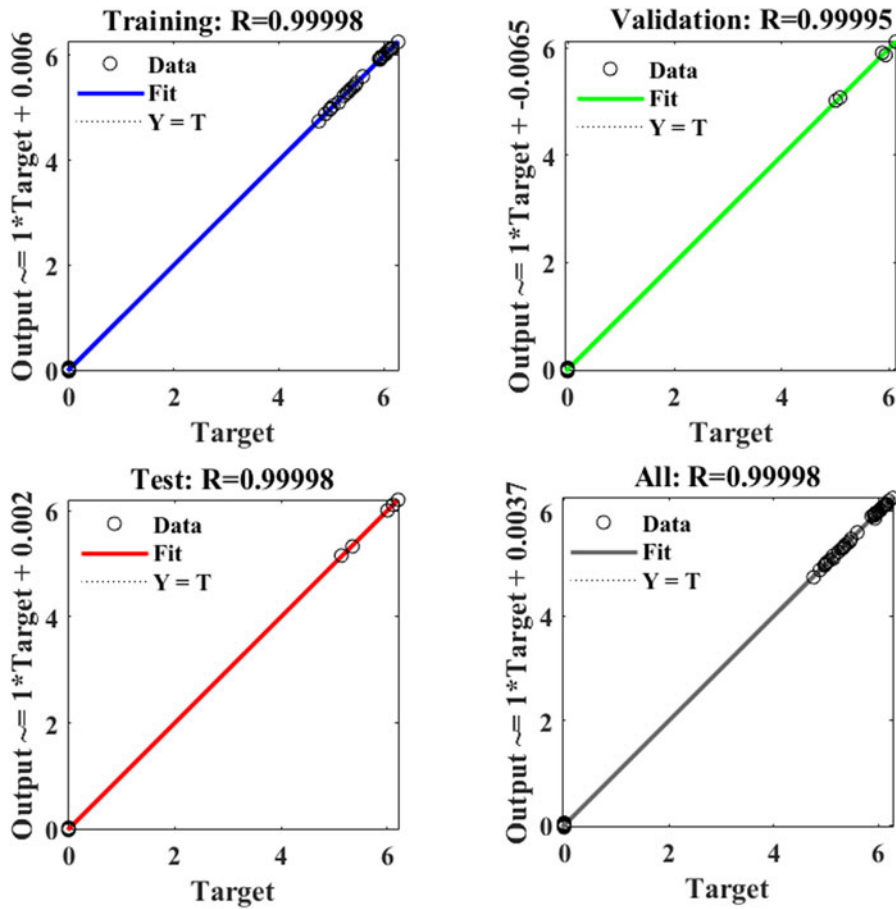


Fig. 10. Regression plot for analyzing the performance of the designed antenna.

Table 3. Absolute error estimation for the analysis of the designed antenna.

Inputs			HFSS outputs				ANN outputs				Absolute error			
c	d	θ	f_{r1}	f_{r2}	f_{r3}	f_{r4}	f_{r1}	f_{r2}	f_{r3}	f_{r4}	f_{r1}	f_{r2}	f_{r3}	f_{r4}
10	2	0	5.086	0	0	0	5.072	-0.003	0.025	-0.014	0.013	0.003	-0.025	0.014
10	3.5	0	4.990	0	0	0	4.991	-0.008	0.008	0.011	-0.001	0.008	-0.008	-0.011
9.5	3	0	5.134	0	0	0	5.152	-0.005	0.008	-0.010	-0.017	0.005	-0.008	0.010
10.5	3	0	4.885	0	0	0	4.882	-0.009	0.017	0.020	0.003	0.009	-0.017	-0.020
10	2.5	30	0	5.399	0	0	-0.009	5.383	-0.019	-0.021	0.009	0.016	0.019	0.021
10	3.5	30	0	5.343	0	0	-0.006	5.323	-0.023	-0.016	0.006	0.019	0.023	0.016
9	3	30	0	5.600	0	0	0.012	5.598	-0.005	0.0006	-0.012	0.001	0.005	-0.000
11	3	30	0	5.142	0	0	0.012	5.101	-0.034	-0.009	-0.012	0.041	0.034	0.009
10	2	60	0	0	6.002	0	-0.001	-0.003	6.002	-0.0001	0.001	0.003	-0.000	0.000
10	3	60	0	0	5.945	0	-0.005	-0.022	5.972	0.008	0.005	0.022	-0.026	-0.008
9	3	60	0	0	6.106	0	0.007	-0.006	6.114	0.014	-0.007	0.006	-0.007	-0.014
10.5	3	60	0	0	5.873	0	-0.017	-0.025	5.909	0.009	0.017	0.025	-0.036	-0.009
10	3.5	90	0	0	0	6.106	-0.017	-0.010	-0.026	6.105	0.017	0.010	0.026	0.000
10	4	90	0	0	0	6.074	-0.012	-0.004	-0.026	6.079	0.012	0.004	0.026	-0.005
9.5	3	90	0	0	0	6.202	-0.008	-0.009	-0.028	6.202	0.008	0.009	0.028	0.000
11	3	90	0	0	0	5.929	-0.003	-0.010	-0.050	5.920	0.003	0.010	0.050	0.009
Average absolute error											0.045	0.191	0.084	0.012

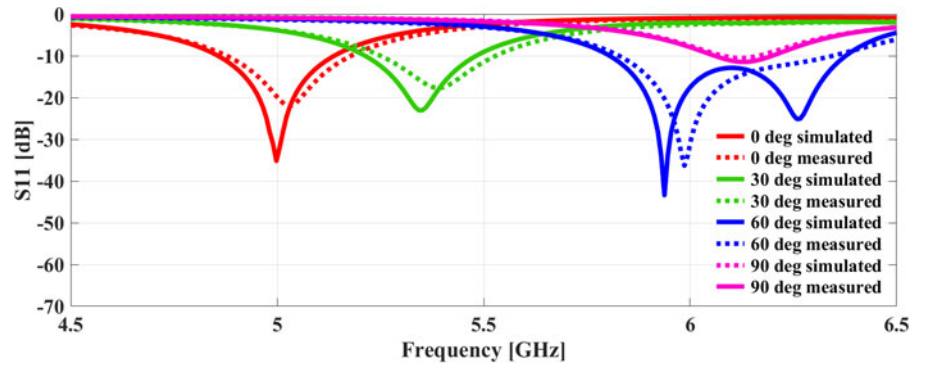


Fig. 11. Simulated (solid line) and measured (dotted line) S11 of the designed antenna.

Table 4. Summarized results of the designed antenna.

Orientation angle	Simulated		Measured	
	Resonant frequency (GHz)	Return loss	Resonant frequency (GHz)	Return loss
0°	4.99	-35.1748	5.03	-21.9950
30°	5.35	-23.0528	5.39	-17.7132
60°	5.93	-43.3927	5.98	-36.3314
90°	6.12	-10.5187	6.13	-11.4674

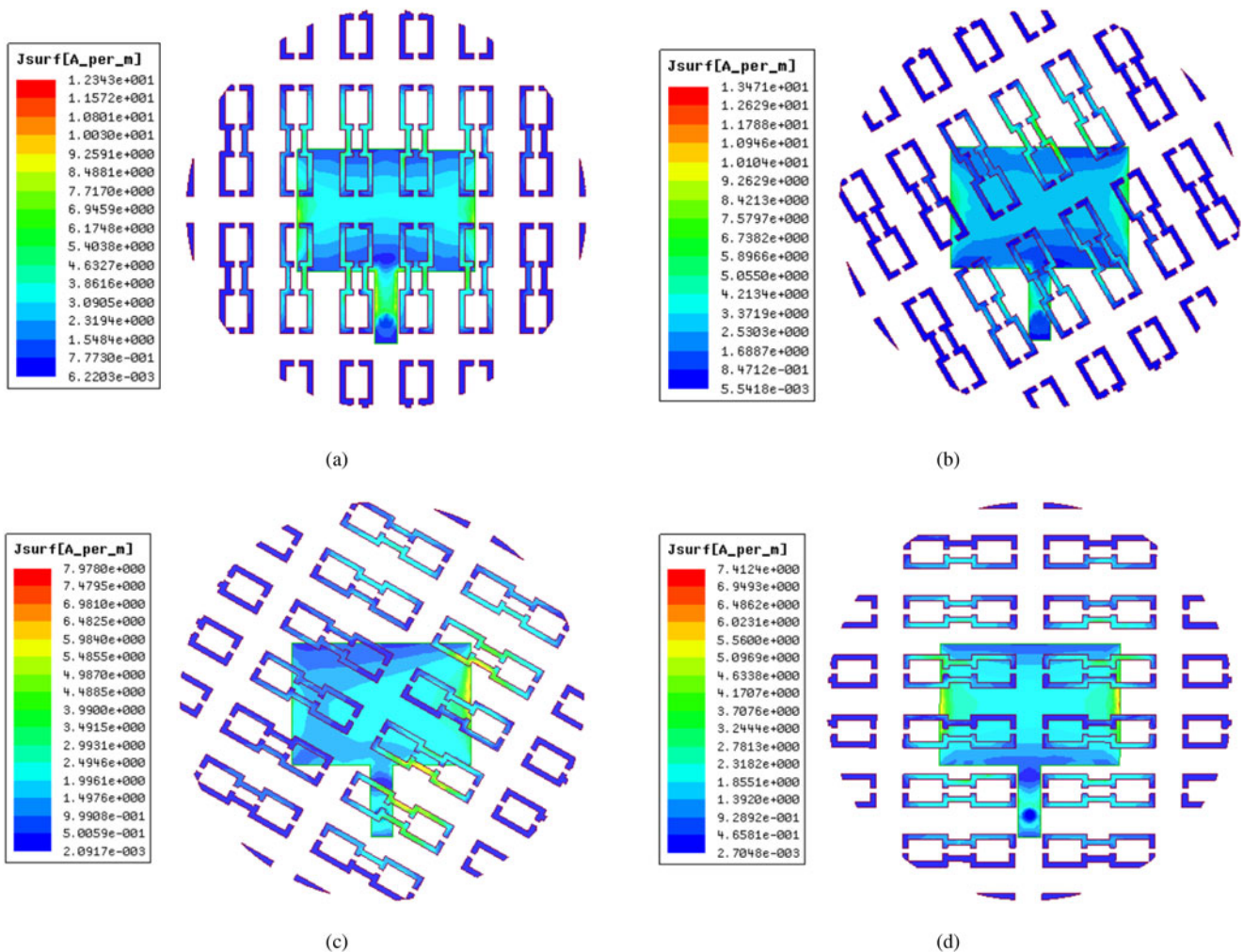


Fig. 12. Surface current distribution obtained at orientation angles (a) 0° (b) 30° (c) 60°, and (d) 90°

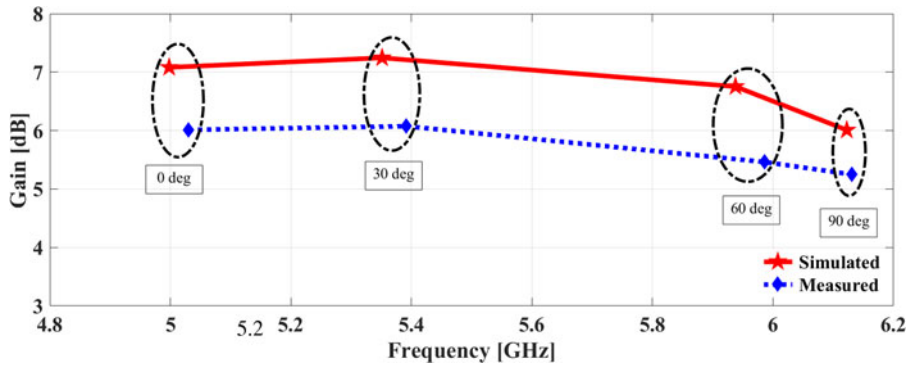


Fig. 13. Simulated and measured gain at different orientation angles.

Regression analysis is a statistical measure for examining and comprehending the relationship between target and output values. Its value should be close to 1 for getting a good performance results. The regression plot showing the performance analysis during training, validation, and testing is shown in Fig. 10. The total regression value of 0.99998 is obtained. The absolute error estimation for analyzing the designed antenna is shown in Table 3. It contains 16 samples that are randomly selected from the generated data set. The average absolute error estimated for f_{r1} , f_{r2} , f_{r3} , and f_{r4} are 0.045, 0.191, 0.084, and 0.012, respectively.

Reflection coefficient

The simulated and measured values of S11 of the designed antenna are illustrated in Fig. 11. Both the results are in good accord. It is anticipated from Fig. 11 that by rotating the metasurface from 0° toward 30°, 60° and 90° with reference to the stationary patch antenna, the resonant frequency continuously shifts up from 4.99 to 5.35, 5.93, and 6.12 GHz, respectively. The best match occurs at an orientation angle corresponding to 60°. After further rotation of the metasurface, the matching decays. Thus, the metasurface plays an integral role in achieving the frequency reconfiguration property. Table 4 shows the summarized results of the proposed antenna with respect to different orientation angles. Slight disagreement is there between the simulated and measured results. This dissimilarity is basically due to the soldering bumps, fabrication, and measurement tolerances.

Current distribution

The surface current distribution at different orientation angles is depicted in Fig. 12. It has been elucidated from these figures that the current distribution is intensively concentrated near the center of the metasurface and edges of the patch at 0° orientation angle. At 30° orientation angle, the distribution is strong across the right-portion of metasurface and left/right edge of the patch. More current flows near the extreme right part of both metasurface and patch corresponding to 60° orientation angle. In the case of 90° orientation angle, the current distribution is intensively accumulated along the center of the metasurface and edges of the patch.

Gain

Gain is an important performance parameter that describes how efficiently information is to be sent or received by an antenna in a particular direction [39]. The simulated and measured gain



Fig. 14. Designed antenna in an anechoic chamber.

obtained at orientation angles corresponding to 0, 30, 60, and 90° [20] is presented in Fig. 13.

Radiation pattern

Figure 14 shows the designed antenna placed in an anechoic chamber. The 2D simulated and measured radiation characteristics of an antenna analyzed at resonant frequencies corresponding to different orientation angles are shown in Fig. 15. These patterns are defined for both the principal planes ($\varphi = 0^\circ$ and $\varphi = 90^\circ$). At $\varphi = 0^\circ$, the pattern exhibited by the antenna is bidirectional and $\varphi = 90^\circ$, the radiation pattern obtained is omnidirectional in shape. The radiation pattern plots indicate that the co-polarization observed along the y -axis radiates highly as compared to the cross-polarization that is observed along the x -axis. The value of the front-to-back ratio examined is also more than 20 dB at all orientation angles. Thus, the metasurface only reconfigures the operating frequency of an antenna without much affecting the shape of the radiation pattern and polarization at different orientation angles.

Table 5 compares the performance parameters of the proposed work with other existing frequency reconfigurable antennas. It is apparent from Table 5 that the proposed antenna achieves 19, 88.2, 48.16, and 48.16% reduction in size as compared to [20], [21], [41] and [25], respectively. On considering the bandwidth, it is observed that 50.66 and 169% hike as compared to [20] and [40], respectively. The comparative tuning range of the proposed antenna with other research in Table 5 indicates a 6.3 1.3, 6.3% rise in tuning range as compared to recent research in

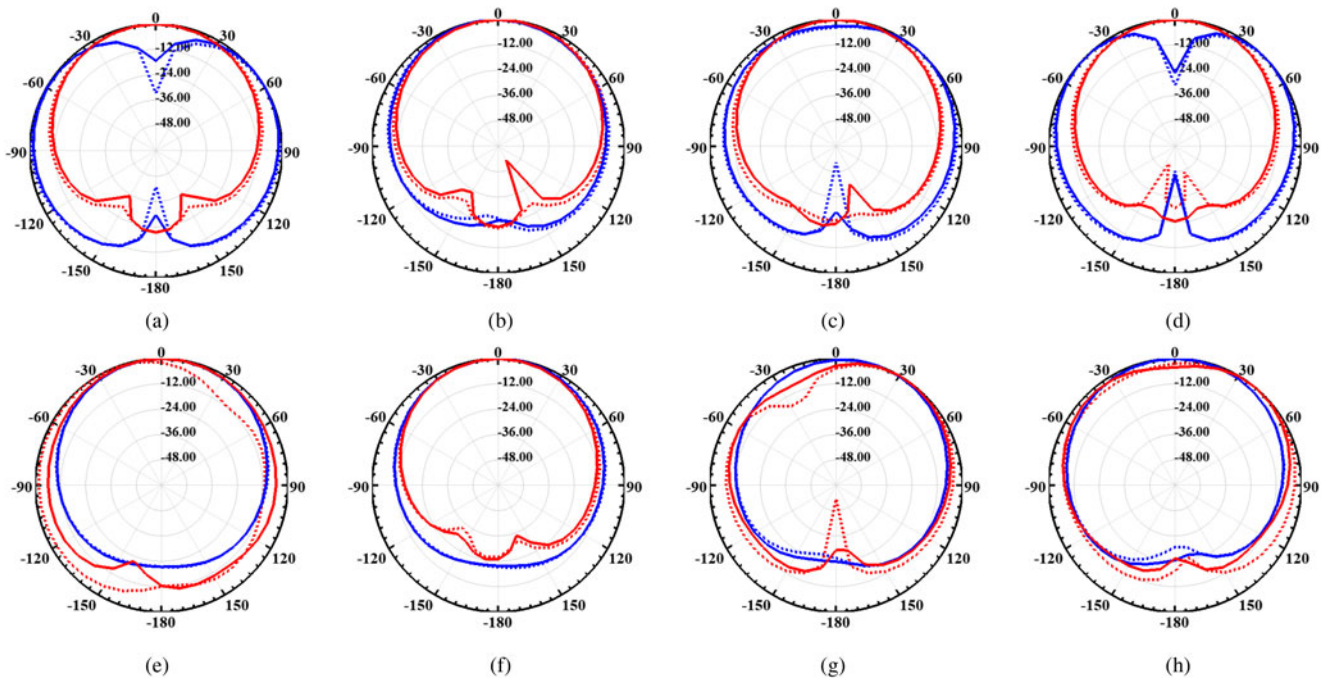


Fig. 15. Simulated (solid line) and measured (dotted line) radiation pattern of FRPA-MSS at orientation angles (a) 0° (b) 30° (c) 60° (d) 90° in x - z plane and in y - z plane (e) 0° (f) 30° (g) 60° (h) 90°.

Table 5. Comparison of proposed work with other existing frequency reconfigurable antennas.

	[20]	[21]	[40]	[24]	Proposed work
Size	40 mm	105 mm × 105 mm	50 mm	50 mm	36 mm
Electrical size	0.67 λ	0.735 λ × 0.735 λ	0.5 λ	–	0.66 λ
Operating frequency	5 GHz	–	3 GHz	–	5.55 GHz
Antenna	Patch	Slot	Slot	Slot	Patch
Metasurface	Rectangular loop unit cells	Meandered unit cells	Rectangular loop unit cells	Ellipse type and wire type unit cells	CDSRR unit cells
Tuning range	4.76–5.51 GHz	1.9–2.3 GHz	2.78–3.2 GHz	3.97–4.74 GHz and 3.84–4.55 GHz (ellipse) and 3.82–4.87 GHz (wire)	4.99–6.12 GHz
Bandwidth	750 MHz	–	420 MHz	–	1.13 GHz
Fractional tuning range	14%	19%	14%	21.1%, 18.9% (ellipse) and 24.2% (wire)	20.3%
Gain	5 dBi	5 dBi	4.8 dBi	–	> 6 dB
Technique used	–	–	–	Radially homogenous model	ANN

[20], [21], and [40], respectively. It can be examined from the comparison that the proposed antenna possesses smaller dimensions with acceptable gain, wide bandwidth, and tuning range at all orientation angles.

Conclusion

In this paper, the design of FRPA-MSS using the ANN has been proposed and investigated. The compounded double split ring-shaped resonator unit cells arranged periodically forming the metasurface are mounted atop the superstrate layer for

accomplishing the desired tuning range. By mechanically tuning the metasurface with respect to the reference patch antenna, frequency reconfiguration is achieved within the 4.99–6.12 GHz tuning range. A good correlation is seen between the measured results and simulated predictions. Also, the proposed antenna owns wide bandwidth and acceptable gain at all orientation angles. The developed ANN model demonstrates its utility for the prediction of resonant frequencies at different orientation angles.

Acknowledgement. The authors would like to thank Rogers Corporation for providing support material for fabricating the antenna prototype and the

National Institute of Technical Teachers Training and Research (NITTTR), Chandigarh, and the Indian Institute of Technology (IIT), New Delhi for providing the facility to test the fabricated prototype.

References

- Chandra KV, Satyanarayana M and Battula KT (2019) A novel miniature hexagonal shape switched pattern and frequency reconfigurable antenna. *International Journal of Communication Systems* **33**(5), 1–8.
- Dwivedy B, Behera SK and Singh V (2018) A versatile triangular patch array for wideband frequency alteration with concurrent circular polarization and pattern reconfigurability. *IEEE Transactions on Antennas and Propagation* **67**(3), 1640–1649.
- Zhu HL, Cheung SW and Yuk TI (2015) Mechanically pattern reconfigurable antenna using metasurface. *IET Microwaves, Antennas & Propagation* **9**(12), 1331–1336.
- Yashchyshyn Y (2010) Reconfigurable antennas: the state of the Art. *INTL Journal of Electronics and Telecommunications* **56**(3), 319–326.
- Iqbal A, Smida A, Abdulrazak LF, Saraereh OA, Mallat NK, Elfergani I and Kim S (2019) Low-profile frequency reconfigurable antenna for heterogeneous wireless systems. *Electronics* **8**(9), 1–11.
- Lim MC, Rahim SKA, Hamid MR, Eteng AA and Jamlos MF (2017) Frequency reconfigurable antenna for WLAN application. *Microwave and Optical Technology Letters* **59**(1), 171–176.
- Kehn MNM, Quevedo-Reruel O and Rajo-Iglesias E (2011) Reconfigurable loaded planar inverted-f antenna using varactor diodes. *IEEE Antennas and Propagation Letters* **10**, 466–468.
- Zhang C, Yang S, Pan HK, Fathy AE, Ghazaly SE and Nair VK (2009) A reconfigurable multiband patch antenna for wireless applications using MEMS switches. *Microwave and Optical Technology Letters* **51**(8), 1892–1896.
- Liu Q, Wang N, Wu C, Wai G and Smolders AB (2014) Frequency reconfigurable antenna controlled by multi-reed switches. *IEEE Antennas and Wireless Propagation Letters* **14**, 927–930.
- Pendharker S, Shevgaonkar RK and Chandorkar AN (2014) Optically controlled frequency-reconfigurable microstrip antenna with low photoconductivity. *IEEE Antennas and Wireless Propagation Letters* **13**, 99–102.
- Ahmad A, Arshad F, Naqvi SI, Amin Y, Tenhunen H and Loo J (2018) Flexible and compact spiral-shaped frequency reconfigurable antenna for wireless applications. *IETE Journal of Research* **66**(1), 22–29.
- Ouyang W, Vosoughi A and Gong X (2019) A frequency-reconfigurable electronically-steerable parasitic array radiator using microstrip patch antennas. *Microwave and Optical Technology Letters* **62**(3), 1409–1422.
- Kim S, Kuester EF, Holloway CL, Scher AD and Jarvis JB (2011) Boundary effects on the determination of metamaterial parameters from normal incidence reflection and transmission measurements. *IEEE Transactions on Antennas and Propagation* **59**(6), 2226–2240.
- Veselago VG (1968) The electrodynamics of substances with simultaneously negative values of ϵ and μ . *Soviet Physics Uspekhi* **10**(4), 504–514.
- Ali T, Aw MS and Biradar RC (2018) A fractal quad-band antenna loaded with L-shaped slot and metamaterial for wireless applications. *International Journal of Microwave and Wireless Technologies* **10**(7), 826–834.
- Ramachandran T, Faruque MRI and Islam MT (2020) A dual band left-handed metamaterial enabled design for satellite applications. *Results in Physics* **16**, 1–8.
- Luo X (2019) Metamaterials and metasurfaces. *Advanced Optical Materials* **7**, 1900885.
- Haupt RL and Lanagan M (2013) Reconfigurable antennas. *IEEE Antennas and Propagation Magazine* **55**(1), 49–61.
- Glybovski SB, Tretyakov SA, Belov PA, Kivshar YS and Simovski CR (2016) Metasurfaces: from microwaves to visible. *Physics Reports* **634**, 1–72.
- Zhu HL, Liu XH, Cheung SW and Yuk TI (2014) Frequency-reconfigurable antenna using metasurface. *IEEE Transactions on Antennas and Propagation* **62**(1), 80–85.
- Chatterjee J, Mohan A and Dixit V (2018) A novel frequency reconfigurable slot antenna using metasurface. *IEEE Indian Conference on Antennas and Propagation (InCAP)* 16–19th Dec, 2018, Hyderabad, India.
- Majumder B, Krishnamoorthy K, Mukherjee J and Ray KP (2016) Frequency reconfigurable slot antenna enabled by thin anisotropic double layer metasurface. *IEEE Transactions on Antennas and Propagation* **64**(4), 1218–1225.
- Ni C, Chen MS, Zhang ZX and Wu XL (2018) Design of frequency-and-polarization-reconfigurable antenna based on the polarization conversion metasurface. *IEEE Antennas and Wireless Propagation Letters* **17**(1), 78–81.
- Li H, Man X and Qi J (2019) Accurate and robust characterization of metasurface-enabled frequency reconfigurable antennas by radially homogeneous model. *IEEE Access* **7**, 122605–122612.
- Sivia JS, Phawaha APS and Kamal TS (2013) Analysis and design of circular fractal antenna using artificial neural networks. *Progress in Electromagnetics Research B* **56**, 251–267.
- Kaur N, Sivia and JS and Rajni (2021) Metasurface incorporated frequency reconfigurable planar antenna for wireless applications. *Progress in Electromagnetics Research C* **113**, 265–275.
- Kaur N, Sivia and JS and Rajni (2021) Artificial neural network based metasurface inspired planar frequency reconfigurable antenna for wireless applications. *International Journal of RF and Microwave Computer-Aided Journal* **31**(9), 1–13.
- Rajni and Marwaha A (2015) Magnetic resonance in spiral resonators. *International Journal of Applied Engineering Research*. **10**(13), 33291–33295.
- Sharma N and Bhatia SS (2019) Double split labyrinth resonator-based CPW-fed hybrid fractal antennas for PCS/UMTS/WLAN/Wi-MAX applications. *Journal of Electromagnetic Waves and Applications* **33**(18), 2476–2498.
- Rajni R and Marwaha A (2013) Role of geometry of split ring resonators in magnetic resonance of metamaterials. *International Journal of Electronics and Communication Engineering & Technology* **4**(7), 279–285.
- Sethi A and Rajni (2018) Determination of electromagnetic parameters of a new metasurface comprising of square loop. *Journal of Engineering Science and Technology* **13**(1), 048–057.
- Rajni and Marwaha A (2015) Resonance characteristics and effective parameters of new left hand metamaterial. *Telkonnika Indonesian Journal of Electrical Engineering* **15**(3), 497–503.
- Varamini G, Keshtkar A, Daryasafar N and Moghadasi MN (2018) Microstrip Sierpinski fractal carpet for slot antenna with metamaterial loads for dual-band wireless application. *International Journal of Electronics and Communications* **84**, 93–99.
- Bilotti F, Toscano A, Vegni L, Aydin K, Alici KB and Ozbay E (2007) Equivalent-circuit models for the design of metamaterials based on artificial magnetic inclusions. *IEEE Transactions on Microwave Theory and Techniques* **55**(12), 2865–2873.
- Kaur M and Sivia JS (2019) Giuseppe Peano and Cantor set fractals based miniaturized hybrid fractal antenna for biomedical applications using artificial neural network and firefly algorithm. *International Journal of RF and Microwave Computer-Aided Engineering* **30**(2), 1–11.
- Kaur M and Sivia JS (2020) ANN and FA based design of hybrid fractal antenna for ISM band applications. *Progress in Electromagnetics Research C* **98**, 127–140.
- Kaur M and Sivia JS (2019) ANN-based design of hybrid fractal antenna for biomedical applications. *International Journal of Electronics* **106**(8), 1184–1199.
- Kaur M and Sivia JS (2019) Minkowski, Giuseppe Peano and Koch curves based design of compact hybrid fractal antenna for biomedical applications using ANN and PSO. *International Journal of Electronics and Communications* **99**, 14–24.
- Balanis CA (2005) *Antenna Theory: Analysis and Design*. Hoboken, NJ: John Wiley & Sons.
- Zhu HL, Cheung SW, Liu XH, Cao YF and Yuk TI (2005) Frequency reconfigurable slot antenna using metasurface. The 8th European Conference on Antennas and Propagation (EuCAP), April 2014, The Hague, Netherlands, pp. 2575–2577.



Ms. Navneet Kaur obtained his bachelor' (B.Tech.) in electronics and instrumentation engineering from Punjab Technical University, Jalandhar and master' (M.Tech.) in electronics and communication engineering from Punjabi University Patiala, Punjab, India in 2005 and 2007, respectively. She is currently working toward the Ph.D. degree in electronics and communication engineering (ECED) from Punjabi

University Patiala, Punjab, India. She has published more than 10 research papers in several international journals, international and national conferences. Her current research interests include microstrip antennas, artificial neural networks, and reconfigurable antennas in wireless communication systems.



Dr. Jagtar Singh Sivia born in Bathinda, Punjab in 1976. He has obtained his B.Tech from Punjab Technical University, Jalandhar, Punjab in electrical and electronics communication engineering in 1999 and he had obtained his master's from Punjab Technical University, Jalandhar in 2005. He obtained his Ph.D. degree from Sant Longowal Institute of Engineering and Technology, Longowal, Punjab. Currently,

he is a professor in electronics and communication engineering at

Yadavindra College of Engineering, Off-Campus of Punjabi University, Patiala, Punjab, India. He has published more than 60 papers in several international journals and international and national conferences. His main interests are in neural networks, electromagnetic waves, genetic algorithms, antenna system engineering. Mr. Sivia is a member of Institution of Engineers in India, Indian Society of Technical Education and International Association of Engineers.



Dr. Rajni is currently professor at Shaheed Bhagat Singh State University (formerly known as Shaheed Bhagat Singh State Technical Campus) Ferozepur, India. She has done her B.Tech. from National Institute of Technology (formerly known as Regional Engineering College) Kurukshetra and M.E. from National Institute of Technical Teacher Training and Research (NITTTR), Chandigarh.

She did her Ph.D. in metamaterial antennas from Sant Longowal Institute of Engineering and Technology, Longowal (SLIET), Sangrur, Punjab. She has approximately 23 years of academic experience. She has authored more than 80 papers in international journals, national and international conferences. Her research interests include wireless communication, antenna design and signal processing.